A Series of Centrifuge Experiments Investigating the Effect of High Confining Pressure on Sand liquefaction

Min Ni, M.S. [1], Tarek Abdoun, PhD, M.ASCE [2],
Ricardo Dobry, PhD, M.ASCE[3] and Waleed El-Sekelly, PhD, PE[4]

[1]Graduate Research Assistant, Department of Civil and Environmental Engineering, Rensselaer Polytechnic Institute, 110 8th St, Troy, NY; e-mail: nim@rpi.edu
[2]Professor, Department of Civil and Environmental Engineering, Rensselaer Polytechnic Institute, 110 8th St, Troy, NY; e-mail: abdout@rpi.edu
[3]Professor, Department of Civil and Environmental Engineering, Rensselaer Polytechnic Institute, 110 8th St, Troy, NY; e-mail: dobryr@rpi.edu
[4] Lecturer, Dept. of Structural Eng., Mansoura University, Mansoura, Egypt and Research Scientist at New York University Abu Dhabi, Abu Dhabi, United Arab Emirates; e-mail: welsekelly@mans.edu.eg

ABSTRACT
This paper introduces a series of centrifuge tests -under low and high confining pressures- designed to study the effect of effective overburden pressure on liquefaction potential of clean sand. All the centrifuge tests simulate about 5m saturated clean sand deposit under effective overburden pressure of 1 and 6 atm with relative density ranging from 45% to 80%. To achieve the targeted overburden pressures, a dry layer of lead shots with different thickness was deposited on top of the clean sand. Viscous fluid was used for saturation to keep constant prototype permeability. All the centrifuge tests were subjected to 10-cycle sinusoidal seismic motions with different prototype peak acceleration to achieve the targeted maximum excess pore pressure buildup. Acceleration, pore pressure build-up and dissipation, and shear wave velocity were monitored, recorded and analyzed during or after shaking. Acceleration amplification was observed in experiments conducted under low confining pressures, while de-amplification was found in experiments conducted under high confining pressures.

INTRODUCTION
Liquefaction is one of the main reasons for the life and property losses during earthquake events, and one of the most complicated and important issues in geotechnical field (Chen et al. 2008). Severe earthquakes are still a big concern nowadays, such as the 1964 Niigata Earthquake (Ishihara and Koga 1981), the 1971 San Fernando earthquake hitting the San Fernando dam, the 2008 Wenchuan Earthquake of magnitude 8.0, the 2011 Great East Japan Earthquake in the Tokyo Bay Area, the Mw 8.1 2017 Chiapas Mexico Earthquake, and the 2018 magnitude 7.5 Palu earthquake. All of these liquefaction-inducing earthquakes have attracted extensive attention from researchers as well as practice engineers (Sharp et al. 2003; Huang & Yu, 2013). Seed and Idriss (1971) proposed the simplified method for field liquefaction triggering evaluation, and after that, a large amount of work has been devoted to it. In their method, the cyclic stress ratio (CSR) is evaluated mainly based on the maximum ground acceleration while the cyclic resistance ratio (CRR) is evaluated based on field tests, such as the cone penetration

test, the standard penetration test, or the shear wave velocity (Youd 2001; Cetin et al. 2004; Idriss and Boulanger 2006, 2008, 2010; Boulanger et al. 2011; Boulanger and Idriss 2012; Robertson and Wride 1998; Andrus and Stokoe 2000). Liquefaction occurs when CSR is larger than CRR.

Figure 1 shows one of the State of Practice (SOP) charts for liquefaction triggering evaluation based on the cone penetration test (CPT). The semi-empirical liquefaction-evaluation chart in Figure. 1 was based on case histories, where the liquefiable sand layers were under effective overburden pressure less than 1.5 atm (low overburden pressure) (Dobry and Abdoun, 2015). However, there are still some important projects, like earth dams that are under high confining pressure of larger than 2 atm, or even higher than 10 atm (Gillette 2013). One of the field case examples is the failure of the upstream slope of the Lower San Fernando Dam, in California, due to liquefaction during the 1971 San Fernando earthquake (Figure 2).

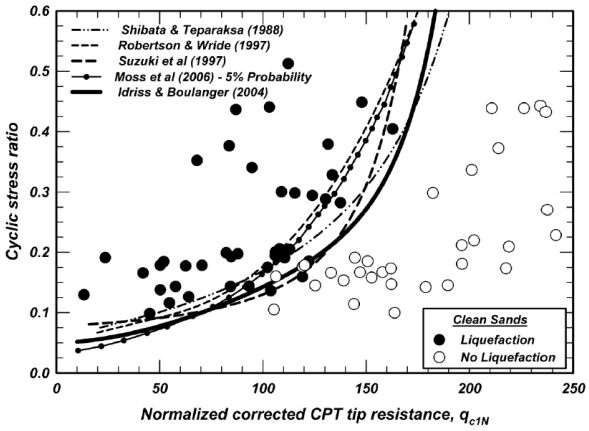

Figure 1. CPT-based field liquefaction chart for clean sands for M = 7.5 and σ′v0 = 1 atm (Idriss and Boulanger 2008)

Figure 2. Lower San Fernando dam after the San Fernando earthquake (1971) (Courtesy of the National Information Service for Earthquake Engineering, EERC, University of California, Berkeley)

To account for the effect of overburden pressure on CRR, Seed (1983) defined the overburden pressure factor (Kσ) as the ratio of CRR at σ'vc to the CRR at σ'vc=1 atm with the same relative density (DR). After that, many researchers came up with Kσ correlations and produced Kσ charts to be used by practitioners (Hynes and Olsen, 1999; Youd et al., 2001; Boulanger and Idriss, 2004). Among them, the two most popular state of practice methods for Kσ estimation are that produced by Youd et al. (2001) and Boulanger and Idriss (2004). However, the effect of overburden pressure on CRR has never been evaluated with centrifuge experiments, one of the techniques closest to field situations (Joseph et al. 1988). This paper introduces a series of centrifuge tests of various effective overburden pressures and relative densities conducted at Rensselaer Polytechnic Institute (RPI), designed to study the effect of overburden pressure. Multiple data sets of centrifuge tests were recorded with various instrumentations.

EXPERIMENTAL PROGRAM

A series of four centrifuge tests (Test 45 - 1, Test 45 - 6, Test 80 - 1 and Test 80 - 6) were conducted in the 1-D stacked ring laminar container and shaker of the geotechnical centrifuge facility at RPI to test the effect of high confining pressure on the liquefaction behavior of clean sands. The test label indicates the combination Relative Density (Dr) after spinning to the designated g-level and the vertical effective stress, σ′v0 (e.g., in Test 45 – 1, Dr = 45% and σ′v0 = 1 atm). Figure 3 shows the centrifuge model configuration and setup for Test 45 - 1 and Test 45 - 6.

Model Layout

All the centrifuge models consisted of three distinct layers: the bottom saturated soil deposit layer, the transition coarse sand layer and topped with a lead shot layer, as shown in Figures 3 and 4.

Since laminar container was used to study the topic, a membrane (Figure 4a) was placed inside the container to prevent leaking of saturated sand, and to allow saturation of model deposit.

Ottawa F65 was used to build the sand deposit inside the membrane (Figure 4b). The soil was provided by U.S. Silica, with specific gravity of 2.65. The maximum and minimum void ratios of this sand were measured by GeoTesting Express, with emax = 0.7403 and emin = 0.479. The sand layer was built with dry density of 1602 kg/m3 and 1698 kg/m3 corresponding to relative densities of 45% and 80%, respectively.

The transition layer, placed on top of sand deposit and built after saturation, functioned as a filter between the sand and lead shot layer to prevent the infiltration of heavy lead shot into sand layer (Figure 4c).

The lead shot layer sits on top of the transition layer and also placed after saturation, used to provide high confining pressure to the sand deposit. To achieve 1 atm and 6 atm effective overburden pressure at the middle depth of sand layer, different heights of lead shot were placed accordingly (Figure 4d).

Each centrifuge model was subjected to 1-D 10-cycle sinusoidal shaking applied to the base with a prototype frequency of 2 Hz.

Viscous Fluid

After the sand deposit was dry pluviated, the model was saturated. To keep consistent permeability between model and prototype, the sand model was saturated with viscous fluid of 20 cp or 60 cp viscosity, corresponding to the exact g-level of the centrifuge model. Following the scaling laws, the models simulate the same sand saturated with water in prototype at 20g or 60g centrifugal acceleration, respectively (Taylor, 1995). The viscous fluid was made with water and methylcellulose powder. The saturation procedure follows the standard procedure adopted in previous centrifuge testing at RPI as follows: the laminar container was sealed and a strong vacuum pump was applied to the model; Carbon Dioxide was injected to the model space to replace the remaining air; the above two steps were repeated twice; and finally, viscous fluid was percolated to the sand deposit at a very low rate under vacuum to insure full saturation of the sand model. After saturation, there was an extra 1~2cm of viscous fluid maintained on top of the saturated sand deposit in order to keep the soil deposit fully saturated all the time and saturate transition layer. Finally, the transition layer and lead shot were placed on top.

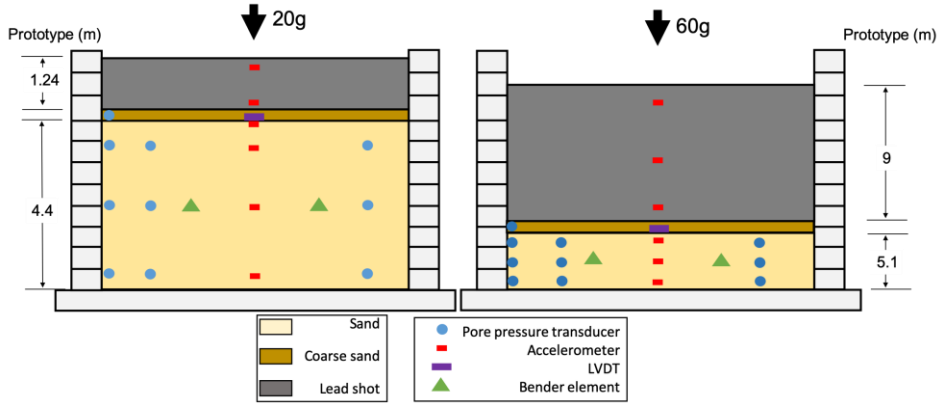

Figure 3. Centrifuge model configuration for two tests with Dr = 45% (Left: 1atm, Right: 6atm)

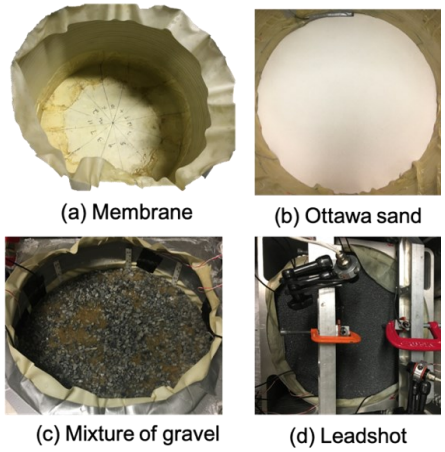

Figure 4. Stages of model building

EXPERIMENTAL RESULTS

Some of the results of the four centrifuge tests are analyzed and presented in this section in prototype scale. Specifically, presented herein are: acceleration time histories, acceleration spectrum, excess pore pressure buildup and dissipation, shear wave velocities, stress-strain loops, and shear modulus degradation curves.

Acceleration Time Histories

Input motions and the corresponding recorded acceleration time histories at different depths of all the four tests are presented in Figure 5. The plots of the same test at different depths are plotted with the same scale to study the change of the acceleration with depth. However, plots of different tests are plotted with different scales for clarity. In Figure 5, the input motion was obtained from the accelerometer attached to the container base, while the acceleration time histories at bottom, middle and top of sand layer were recorded by the accelerometers buried at various depths of saturated sand deposit. Figure 5 demonstrates motion amplification for sand model under low confining pressure (Test 45 - 1 and Test 80 -1), while slight soil de-amplification was observed in the soil deposit under high confining pressure (Test 45 – 6 and Test 80 - 6). Figure 6 shows the response spectrum at the bottom and surface of soil layer. To avoid the effect of motion degradation due to pore pressure build-up, the response spectrum was created based on the first 2 seconds before degradation. According to Figure 6, the primary peaks of the spectrum occur at 2 Hz, which corresponds to the main input acceleration frequency, and the minor peaks before 2 Hz are caused by unavoidable noise, which is ignorable compared with the primary peaks. Figure 6 also shows the amplification under low confining pressure in Test 45 – 1 and Test 80 – 1, and de-amplification under high confining pressure in Test 45 – 6 and Test 80 – 6.

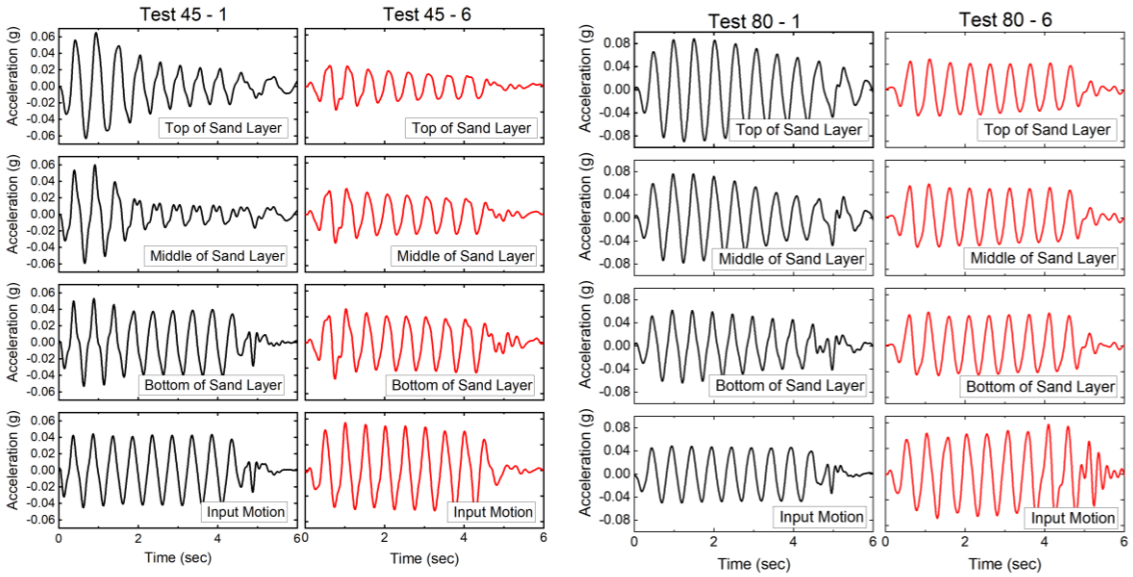

Figure 5. Input motion and acceleration time histories at various depths (Dr = 45% & 80%)

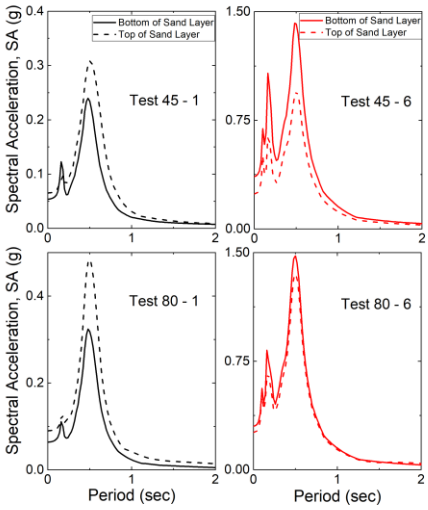

Figure 6. Acceleration at the top of sand layer versus the base acceleration

Excess Pore Pressure Buildup

Figure 7 shows the excess pore pressure ratio time histories during and after shake event for Test 45-1 and 45-6 as well as Tests 80-1 and 80-6. The excess pore pressure ratio was calculated by dividing excess pore pressure, Δu, by the effective vertical stress, σ'v0, at the sensor depth ($r_u = \Delta u / \sigma'_{v0}$). The labels on the figures indicate the relative locations of the pore pressure transducers, consistent with the same location of accelerometers in Figure 5. In all four centrifuge tests with different relative densities and confining pressures, the maximum excess pore pressure ratio increased with depth, that is, the maximum excess pore pressure buildup existed at the bottom depth, closest to the container base. The maximum excess pore pressure ratios of Test 45 – 1, Test 45 – 6 and Test 80 – 1 were around or higher than 0.8, which resulted in degradation of acceleration with time, as shown in Figure 5.

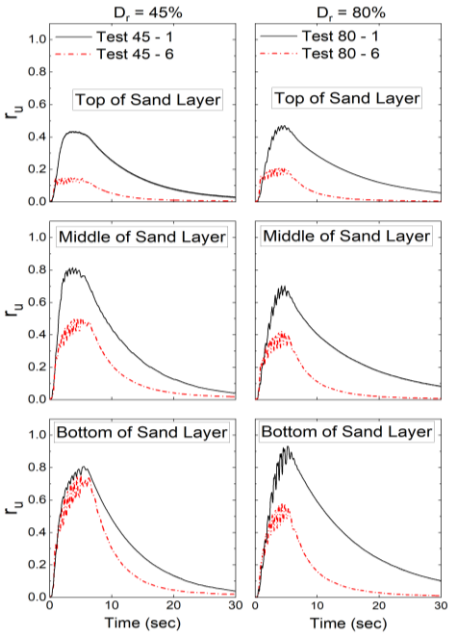

Figure 7. Excess pore pressure ratio time histories during shaking and dissipation at different depths in the soil deposit for all the tests

Shear Wave Velocities

Shear wave velocities, Vs, were obtained for each centrifuge model with different relative densities and confining pressures, using bender elements installed in the mid-depth of the sand deposit (the depth of the targeted effective overburden pressure). Figure 8 shows the measured shear wave velocities of centrifuge tests, the trend lines of shear wave velocities by following Eq. (1).

$$V_s = a(\sigma_0')^{0.25} \quad (1)$$

where σ_0' is the mean effective confining pressure; a is a coefficient -function of void ratio- which is modified in Figure. 8 to fit the shear wave velocity measurements. The coefficient a varies with density, as shown in Fig. 8. The coefficient of lateral stress, K0 =σ'h0/σ'v0 (where σ'h0 and σ'v0 are horizontal and vertical effective stress, respectively) was introduced to calculate the mean effective confining pressure, σ'0 ,

$$\sigma_0' = \frac{1+2K_0}{3}\sigma_{v0}' \quad (2)$$

Herein, K_0 is determined with Eq. (3) (Jaky, 1944)

$$K_0 = 1 - \sin\varphi \quad (3)$$

where φ is the internal friction angle (35° - 38°), determined by El-Sekelly et al. (2014) for similar Ottawa sand with relative density of 45% and 80% using direct shear test.

The comparison results in Figure. 8 demonstrate that the measured shear wave velocities follow the same trend of Eq. (1) (Hardin and Richart, 1963).

Also, the measured ratio in Figure. 8, Vs,80/Vs,45 = 190/166.5 = 1.14. This ratio is compared with Hardin and Richart (1963) and Seed and Idriss (1970) correlation.

According to the prediction by Hardin and Richart Ottawa correlation for G_{max} of rounded sand (Hardin and Richart, 1963):

$$G_{max} = \frac{2630(2.17-e)^2}{1+e}\sqrt{\bar{\sigma}_0} \quad \text{(psi)} \quad (4)$$

So, for the same $\bar{\sigma}_0$:

$$\frac{G_{max80}}{G_{max45}} = \frac{(2.17-e_{80})^2}{(2.17-e_{45})^2}\cdot\frac{1+e_{45}}{1+e_{80}} \quad (5)$$

Where e_{80}=0.53; e_{45}=0.62. Therefore,

$$\frac{G_{max80}}{G_{max45}} = \frac{(2.17-0.53)^2}{(2.17-0.62)^2}\cdot\frac{1+0.62}{1+0.53} = 1.185 \quad (6)$$

But,

$$G_{max} = \rho V_s^2 \Rightarrow V_s = \sqrt{\frac{G_{max}}{\rho}} = \sqrt{\frac{G_{max}\cdot g}{(\rho\cdot g)_{sat}}} \quad (7)$$

$$(\rho\cdot g)_{sat} = \frac{G+e}{1+e}(\rho\cdot g)_{water} \quad (8)$$

Using G = 2.65 for specific gravity.

$$(\rho \cdot g)_{sat} = \frac{2.65+e}{1+e}(\rho \cdot g)_{water} \tag{9}$$

$$\frac{(\rho \cdot g)_{sat80}}{(\rho \cdot g)_{sat45}} = \frac{2.65+e_{80}}{2.65+e_{45}} \cdot \frac{1+e_{45}}{1+e_{80}} \tag{10}$$

So,

$$\frac{V_{s80}}{V_{s45}} = \sqrt{\frac{G_{max80}}{G_{max45}} \cdot \frac{(\rho \cdot g)_{sat45}}{(\rho \cdot g)_{sat80}}} = \sqrt{(1.185) \cdot \frac{2.65+e_{45}}{2.65+e_{80}} \cdot \frac{1+e_{80}}{1+e_{45}}} \tag{11}$$

$$\frac{V_{s80}}{V_{s45}} = \sqrt{(1.185) \cdot \frac{2.65+0.62}{2.65+0.53} \cdot \frac{1+0.53}{1+0.62}} = \sqrt{1.185 \cdot 1.03 \cdot 0.94} = 1.07 \tag{12}$$

According to the prediction by Seed and Idriss (1970) correlation of Gmax versus Dr:

$$G_{max} = 1000 K_{2max} \sqrt{\bar{\sigma}_0} \tag{13}$$

($\bar{\sigma}_0$ and in G_{max} psi)

Table 1 Values of K_{2max} (Seed and Idriss, 1970)

D_r(%)	K_{2max}
45	9.4
80	14.0

K2max values for Dr = 80% is obtained by linear interpolation based on Table 1.
So, for the same $\bar{\sigma}_0$:

$$\frac{G_{max80}}{G_{max45}} = \frac{14.0}{9.4} = 1.489 \tag{14}$$

And

$$\frac{V_{s80}}{V_{s45}} = \sqrt{\frac{G_{max80}}{G_{max45}} \cdot \frac{2.65+e_{45}}{2.65+e_{80}} \cdot \frac{1+e_{80}}{1+e_{45}}} = \sqrt{1.489 \cdot 1.03 \cdot 0.94} = 1.20 \tag{15}$$

Thus, the experimental ratio of: $\frac{V_{s80}}{V_{s45}} = 1.14$ is consistent with the range of ratios, 1.07-1.20, obtained from the Hardin and Richart (1963) and Seed and Idriss (1970) correlation.

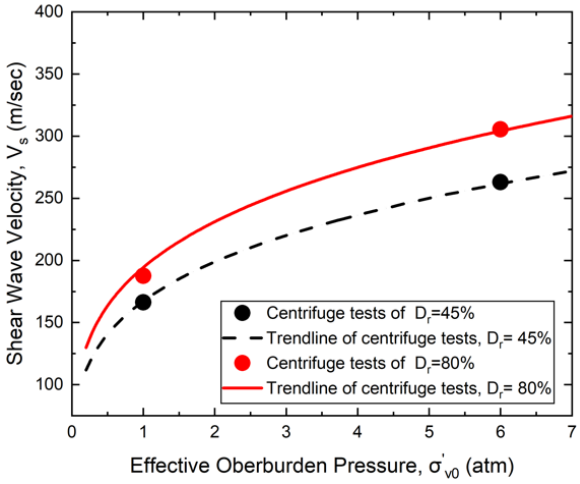

Figure 8. measured shear wave velocities of centrifuge tests and the corresponding trendlines

CONCLUSION

A series of four centrifuge tests (Tests 45-1, 45-6, 80-1 and 80-6) with different relative densities and effective overburden pressures were conducted in order to study the sand behavior under low and high confining pressures. Some of the experimental results were analyzed and demonstrated. A new centrifuge technique was established to provide sand model with various confining pressures with three distinct layers: the saturated sand deposit, the transition layer and the heavy lead shot layer. This technique proved successful and opens new venues for research at any centrifuge facility. According to the data analysis, amplification of acceleration was observed under low confining pressure in Test 45 - 1 and Test 80 - 1, while de-amplification of acceleration existed in Test 45 – 6 and Test 80 – 6 under high confining pressures. The shear wave velocities measured from bender elements for loose and dense sand models were in good agreement with the formula form of $V_s = a(\sigma_0')^{0.25}$, also validated by literature predictions.

ACKNOWLEDGMENTS

The authors wish to thank the RPI geotechnical centrifuge technical staff for their help in the project and the preparation of this paper. Prof. Mourad Zeghal helped with the system identification of records, which is most appreciated. The research was supported by the National Science Foundation under Grants No. 1545026 & 1904313 and NYU Abu Dhabi; this support is gratefully acknowledged.

REFERENCES

Andrus, R. D., and Stokoe II, K. H. (2000). "Liquefaction resistance of soils from shear-wave velocity." Journal of geotechnical and geoenvironmental engineering, ASCE, 126(11), 1015-1025.

Boulanger, R. W., and Idriss, I. M. (2004). "State normalization of penetration resistance and the effect of overburden stress on liquefaction resistance." Proceedings 11th SDEE and 3rd ICEGE, University of California, Berkeley, CA.

Boulanger, R. W., Wilson, D. W. and Idriss, I. M. (2011). "Examination and reevalaution of SPT-based liquefaction triggering case histories." Journal of geotechnical and geoenvironmental engineering, ASCE, 138(8), 898-909.

Boulanger, R. W., and Idriss, I. M. (2012). "Probabilistic standard penetration test–based liquefaction–triggering procedure." Journal of geotechnical and geoenvironmental engineering, ASCE, 138(10), 1185-1195.

Cetin, K. O., Seed, R. B., Der Kiureghian, A., Tokimatsu, K., Harder Jr, L. F., Kayen, R. E., and Moss, R. E. (2004). "Standard penetration test-based probabilistic and deterministic assessment of seismic soil liquefaction potential." Journal of geotechnical and geoenvironmental engineering, ASCE, 130(12), 1314-1340.

Chen, L., Hou, L., Cao, Z., Yuan, X., Sun, R., Wang, W., ... & Dong, L. (2008). "Liquefaction investigation of Wenchuan earthquake. " 14th World Conf. on Earthquake Engineering.

Dobry, R., and T. Abdoun. "3rd Ishihara Lecture: An investigation into why liquefaction charts work: A necessary step toward integrating the states of art and practice." Soil Dynamics and Earthquake Engineering 68 (2015): 40-56.

El-Sekelly, W., Tessari, A., and Abdoun, T. (2014). "Shear wave velocity measurement in the centrifuge using bender elements." Geotechnical Testing Journal, 37(4), 689-704.

Gillette, D. (2013). "Liquefaction issues for dam safety - Bureau of Reclamation." Presentation in One-Day Workshop, Committee on State of the Art and Practice in Earthquake Induced Soil Liquefaction Assessment, National Research Council of the National Academies, Washington, DC, November 12.

Hardin, B. O., and Richart Jr., F. E. (1963). "Elastic wave velocities in granular soils." J. Soil Mech. Found. Div., ASCE, 89(1), 33–65.

Huang, Y., & Yu, M. (2013). "Review of soil liquefaction characteristics during major earthquakes of the twenty-first century. " Natural hazards, 65(3), 2375-2384.

Hynes, M. E., Olsen, R. S., and Yule, D. E. (1999). "Influence of confining stress on Liquefaction Resistance." Proc., Int. Workshop on Phys. and Mech. of Soil Liquefaction, Balkema, Rotterdam, The Netherlands, 145–152.

Idriss, I. M., and Boulanger R. W. (2006). "Semi-empirical procedures for evaluating liquefaction potential during earthquakes." Soil Dynamics and Earthquake Engineering, 26(2-4), 115-130.

Idriss, I. M., and Boulanger, R. W. (2008). "Soil liquefaction during earthquakes." Monograph MNO-12, Earthquake Engineering Research Institute, Berkeley, CA.

Idriss, I. M., and Boulanger, R. W. (2010). "SPT-based liquefaction triggering procedures." Report UCD/CGM-10/02, Dept. of Civil and Environmental Engineering, Univ. of California, Davis, CA.

Jaky, J. (1944). "The coefficient of earth pressure at rest." J. Soc. Hung. Eng. Arch. (Magyar Mernok es Epitesz-Egylet Kozlonye), 355–358.

Joseph, P. G., Einstein, H. H., and Whitman, R. V. (1988). "A literature review of geotechnical centrifuge modeling with particular emphasis on rock mechanics." MIT Report to the Air Force Engineers and Service Center, Accession No. ADA213793, Tyndall Air Force Base, FL.

Robertson, P. K., and Wride, C. E. (1998). "Evaluating cyclic liquefaction potential using the cone penetration test." Canadian Geotechnical Journal, 35(3), 442-459.

Seed, H. B. "Earthquake-resistant design of earth dams." Proc., Symp. Seismic Des. of Earth Dams and Caverns, ASCE, New York, (1983) 41–64.

Seed, H. B., and Idriss, I. M. (1970). "Analyses of ground motions at Union Bay, Seattle during earthquakes and distant nuclear blasts." Bulletin of the Seismological Society of America, 60(1), 125-136.

Seed, H. B., and I. M. Idriss. "Simplified procedure for evaluating soil liquefaction potential." Journal of Soil Mechanics & Foundations Div (1971).

Sharp, M. K., Dobry, R., & Abdoun, T. (2003). "Liquefaction Centrifuge Modeling of Sands of Different Permeability. " Journal of geotechnical and geoenvironmental engineering, 129(12), 1083-1091.

Taylor, R. N. (1995). "Centrifuges in modelling: principles and scale effects." Chapter 2, Geotechnical centrifuge technology, R. N. Taylor, ed., Blackie Academie & Professional, London, 19-33.

Youd, T. L., and Idriss, I. M. (2001). "Liquefaction resistance of soils: summary report from the 1996 NCEER and 1998 NCEER/NSF workshops on evaluation of liquefaction resistance of soils." Journal of geotechnical and geoenvironmental engineering, ASCE, 127(4), 297-313.